CHEMISTRY OF MATERIALS
Article

Chem. Mater. **2010,** *22,* 2995–2999 2995
DOI:10.1021/cm1004054

Optimizing Thermoelectric Efficiency in $La_{3-x}Te_4$ via Yb Substitution

Andrew F. May,*[,†] Jean-Pierre Fleurial,[‡] and G. Jeffrey Snyder[§]

[†]*Department of Chemical Engineering, California Institute of Technology, Pasadena, California 91125,* [‡]*Jet Propulsion Laboratory, California Institute of Technology, Pasadena, California 91109, and* [§]*Department of Materials Science, California Institute of Technology, Pasadena, California 91125*

Received February 8, 2010. Revised Manuscript Received April 1, 2010

A low temperature, solid state synthesis technique has enabled the production of homogeneous samples of $La_{3-x-y}Yb_yTe_4$. This allows the substitution of divalent Yb to be utilized to optimize the thermoelectric performance in lanthanum telluride. The addition of Yb^{2+} changes the electrical transport properties in a manner that can be well understood using valence counting rules and a corresponding change in the Fermi energy. The substitution of Yb^{2+} for La^{3+} results in a threefold finer control over the carrier density n, thus allowing the optimum $n \sim 0.3 \times 10^{21}$ cm^{-3} to be both predicted and prepared. The net result is an improvement in thermoelectric efficiency, with zT reaching ~1.2 at 1273 K.

Introduction

Thermoelectric power generation has been critical for the exploration of deep space, where generator lifetime is paramount. Historically, such missions have utilized Si−Ge alloys for thermoelectric power generation at high temperatures (> 1000 K). Lanthanum telluride ($La_{3-x}Te_4$, $0 \le x \le 1/3$) is a candidate material to replace SiGe because of its higher thermoelectric efficiency above 1000 K and mechanical properties that are more suitable for integration with other modern thermoelectric materials.[1] Recently, nanostructured SiGe has also demonstrated larger thermoelectric efficiency than observed in traditional SiGe.[2] While SiGe can be doped *n* or *p*-type, $La_{3-x}Te_4$ is inherently *n*-type, and a suitable *p*-type material is required for device development; in 2006, *p*-type $Yb_{14}MnSb_{11}$ was identified as a complementary material.[3]

The high temperature synthesis of $La_{3-x}Te_4$ is complicated by the phase diagram as well as sensitivity to oxygen. For instance, the melting point of $La_{3-x}Te_4$ (~1775 K) is higher than the boiling point of tellurium (~1260 K), and peritectic and eutectic reactions exist with the neighboring $LaTe_2$ and LaTe phases, respectively.[4] Early work exploring the optimization of thermoelectric efficiency in $La_{3-x}Te_4$ utilized high-temperature melt techniques and were hampered due to the frequent production of multiphase, inhomogeneous samples. Mechanical alloying allows the kinetic barriers to synthesis to be overcome without melting the elements, and thus the woes of solidification-based techniques can be avoided.

Homogeneous samples of $La_{3-x}Te_4$ were reproducibly obtained via mechanical alloying and pressure-assisted sintering.[1] This solid state synthesis technique resulted in a thermoelectric figure of merit $zT = \alpha^2 T/\kappa\rho$ of ~1.1 at 1273 K for a Hall carrier density of $n_H \sim 0.5 \times 10^{21}$ cm^{-3}.[1] Here, α is the Seebeck coefficient, ρ the electrical resistivity, and κ the thermal conductivity. The high thermoelectric performance of lanthanum telluride arises from a favorable band structure[5] in combination with a low lattice thermal conductivity, which is the result of a fairly large unit cell and the scattering of phonons via La vacancies.[6−8] An empirical model based on a wide range of compositions suggested an optimization of zT near $x \sim 0.27$, or $n \sim 0.9 \times 10^{21}$ cm^{-3}. However, few samples were prepared near this optimum composition, and the optimization was not fully explored. Early work sponsored by the Jet Propulsion Laboratory suggested that Yb substitution in $La_{3-x}Te_4$ may enhance zT via changes to the effective mass, as in isostructural $La_{3-y}Yb_yS_4$.[9]

In $La_{3-x}Te_4$, the chemical control of carrier density is dictated by the formal valence of lanthanum. Each lanthanum (La^{3+}) releases three electrons to the crystal, and every tellurium utilizes two of these to complete valence (Te^{2-}). The chemical/crystal environment can be represented as

$$La^{3+}_{3-x} V_{La,x} Te^{2-}_4 e^{1-}_{1-3x}$$

*Corresponding author. E-mail: may@caltech.edu.

(1) May, A. F.; Fleurial, J.-P.; Snyder, G. J. *Phys. Rev. B* **2008**, *78*, 125205.
(2) Wang, X. W.; Lee, H.; Lan, Y. C.; Zhu, G. H.; Joshi, G.; Wang, D. Z.; Yang, J.; Muto, A. J.; Tang, M. Y.; Klatsky, J.; Song, S.; Dresselhaus, M. S.; Chen, G.; Ren, Z. F. *Appl. Phys. Lett.* **2008**, *93*, 193121.
(3) Brown, S. R.; Kauzlarich, S. M.; Gascoin, F.; Snyder, G. J. *Chem. Mater.* **2006**, *18*, 1873–1877.
(4) Ramsey, T.; Steinfink, H.; Weiss, E. *Inorg. Chem.* **1965**, *4*, 1154.
(5) May, A. F.; Singh, D. J.; Snyder, G. J. *Phys. Rev. B* **2009**, *79*, 153101.
(6) Toberer, E. S.; May, A. F.; Snyder, G. J. Chem. Mater. **2009**, Article ASAP.
(7) Wood, C. *Rep. Prog. Phys.* **1988**, *51*, 459–539.
(8) Delaire, O.; May, A. F.; McGuire, M. A.; Porter, W. D.; Abernathy, D. L.; Snyder, G. J. *Phys. Rev. B* **2009**, *80*, 184302.
(9) Nakahara, J. F.; Takeshita, T.; Tschetter, M. J.; Beaudry, B. J.; K. A. Gschneidner, J. *J. Appl. Phys.* **1988**, *63*, 2331–2336.

Published on Web 04/14/2010

where V_{La} is a lanthanum vacancy. At $x = 0$, there is thus one free electron per formula unit, and the introduction of lanthanum vacancies removes these conduction electrons until the insulating composition of $x = 1/3$ is reached.[6,7] Therefore, valence counting reveals that the carrier density is related to composition via $n = n_{max}(1 - 3x)$, where $n_{max} \sim 4.5 \times 10^{21}$ cm^{-3} corresponds to $x = 0$.

Finer chemical control over carrier density can be achieved through non-isoelectronic substitutions. For instance, the substitution of a divalent cation M^{2+} for La^{3+} ($La_{3-x-y}M_yTe_4$) results in a local environment of

$$La^{3+}_{3-x-y}V_{La,x}M^{2+}_y Te^{2-}_4 e^{1-}_{1-3x}$$

with a theoretical carrier density of $n = n_{max}(1 - 3x - y)$. Therefore, non-isoelectronic substitutions also provide a way to separate the inherent interdependence of n and vacancy concentration x, thereby allowing physical models of transport to be developed and/or tested. In this study, Yb was selected for the divalent cation because the ionic sizes of Yb^{2+} and La^{3+} are very similar (for the coordination number of eight).[10] This selection also involves consideration of the physical and mechanical properties, as the mechanical alloying synthesis is very sensitive to these basic material properties.

Experimental Methods

In this work, the $La_{3-x-y}Yb_yTe_4$ samples were prepared by mechanical alloying (high energy ball milling) and pressure-assisted sintering (sintering above 1300 K for roughly 3 h), using the same protocols as for $La_{3-x}Te_4$.[1] This synthesis occurs near room temperature by a direct milling of the elements in stainless steel vials. The surfaces of elemental Yb and La chunks are polished prior to cutting, and all steps are performed in an argon glovebox. Milling is completed in less than a day, and a yield of approximately 95% is common for the system of interest. A nonaqueous lubricant is utilized when cutting the samples via a slow speed diamond saw or when polishing the samples for microanalysis.

Phase purity was investigated using powder X-ray diffraction with Cu Kα radiation. Sample homogeneity was inspected via electron probe microanalysis, during which elemental compositions were examined via wavelength dispersive spectroscopy (WDS). The conditions for WDS were identical to those reported in ref 1, with the exception that the data reported for Yb containing samples are an average of many 20 μm WDS scans. $YbPO_4$ was used for the Yb standard.

To analyze the thermoelectric performance, the following properties were measured: thermal diffusivity D_T, Seebeck coefficient α, electrical resistivity ρ, and the Hall coefficient R_H. In summary, D_T is obtained via the laser-flash method (NETZSCH LFA 457), α data are collected by the differential light-pipe method using W/Nb thermocouples, and ρ and R_H are obtained using the van der Pauw technique; see ref 1 for further details. The Hall carrier density is $n_H = 1/R_H e$ where e is the elementary charge; a magnetic field of roughly 2 T was utilized to obtain the Hall data. The thermal conductivity is calculated $\kappa = D_T C_P d$, where d is the density and C_P the heat capacity. The values of C_P were obtained by modifying the C_P of metallic La_3Te_4 ($n_H \sim 4.5 \times 10^{21}$ cm^{-3}) reported in ref 8 to account for the reduced electronic contribution C_{el}. For a conservative modification, the values of $C_{el}(T)$ calculated for La_3Te_4 are scaled by the ratio of room temperature n_H values, and a new heat capacity is obtained for all the samples discussed below. At 300 and 1000 K, C_{el} in the metallic La_3Te_4 is only ~2.6% and 5.8% of the total C_P, respectively.

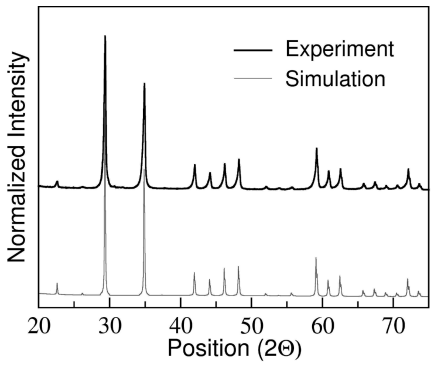

Figure 1. Representative X-ray diffraction scan revealing a nearly single phase sample, with all primary peaks corresponding to the expected Th_3P_4 structure type (simulation curve for comparison). The scan shown corresponds to the sample with $n_H = 0.19 \times 10^{21}$ cm^{-3}.

Results and Discussion

The samples were found to be nearly single phase by X-ray diffraction, as demonstrated by the diffraction scan shown in Figure 1. While all the primary peaks in the diffraction scan can be attributed to the desired Th_3P_4 structure type (space group $I\bar{4}3d$), it is possible minor oxidation occurs as the primary diffraction peaks for the commonly observed La_2O_2Te phase occur near 30° 2Θ. These samples are, however, as phase pure as the lanthanum telluride samples to which they are compared.[1]

The samples appear homogeneous via electron probe microanalysis, where the backscattered electron mode was utilized to investigate compositional fluctuations. An example of one such micrograph is shown in the inset of Figure 2, which shows a homogeneous matrix with some porosity. The image shown is for the same sample with diffraction data presented in Figure 1 ($n_H = 0.19 \times 10^{21}$ cm^{-3} when referencing Table 1). A summary of the wavelength dispersive spectroscopy (WDS) data is shown in Table 1, where changing Yb/La content is observed along with a relatively constant Te content. The variation in Yb/La content is found to trend nicely with the measured carrier density.

Figure 2 shows that the variation of rare earth content does indeed result in the desired control over carrier density, which is assessed via the Hall carrier density n_H. It therefore appears that the Yb content affects n as hypothesized, and n_H will be utilized to examine transport as it is a better characterization of the true n than is n_{WDS}. The values of n_{WDS} were obtained using the WDS data by assuming Yb^{2+} in samples characterized by the formula unit $La_{3-x-y}Yb_yTe_4$. As with previous work,[1] n_{WDS} is larger than expected due to an overestimation of the rare earth content. While quantitative agreement between n_H and n_{WDS} is not obtained, the expected trends are

(10) Shannon, R. D. *Acta Crystallogr.* **1976**, *A32*, 751.

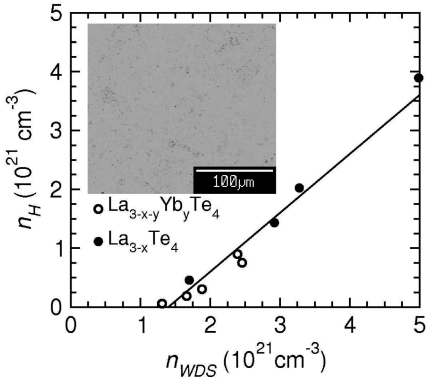

Figure 2. Wavelength dispersive spectroscopy (WDS) data are presented along with the room temperature Hall concentration n_H. The expected correlation between n_H and WDS compositions is qualitatively demonstrated by using valence counting to obtain a carrier density n_{WDS}. The inset shows a representative image taken in backscattered electron mode during electron probe microanalysis, which reveals homogeneous samples with some porosity (the sample corresponds to the X-ray diffraction scan shown in Figure 1).

Table 1. Summary of Wavelength Dispersive Spectroscopy (WDS) Data with Corresponding Room Temperature Hall Density n_H for Each Yb Containing Sample Discussed in This Article

	WDS (atomic percent)		
n_H (10^{21} cm^{-3})	Yb	La	Te
0.06	8.6	34.0	57.4
0.19	7.9	34.8	57.4
0.30	4.4	37.7	57.9
0.75	2.9	39.2	57.8
0.90	2.0	39.9	58.4

observed (a correct slope in the solid line) and are consistent with samples of $La_{3-x}Te_4$, suggesting Yb is indeed primarily divalent. The tuning of Yb content y should therefore render a threefold finer control of n compared to the La vacancy concentration x. The observation of larger than expected rare earth content is believed to be an instrument error associated with the use of oxide standards for La and Yb, though minor oxidation may be present at grain boundaries (not observed experimentally).

The suggestion of Yb^{2+} in the lanthanum telluride matrix is consistent with the general behavior observed in Te-based compounds.[11] This is exemplified by the formation of only YbTe in the Yb−Te phase diagram,[12] which is an insulating phase with divalent Yb.[13,14] Divalent Yb is stabilized due to the full 4f shell, such as in elemental ytterbium[14] where the 4f states lie at binding energies between 1.3 and 2.5 eV.[15] This reasoning is also consistent with the formation of divalent Yb in Yb_4Bi_2Te,[16] which possesses the anti-Th_3P_4 structure type.

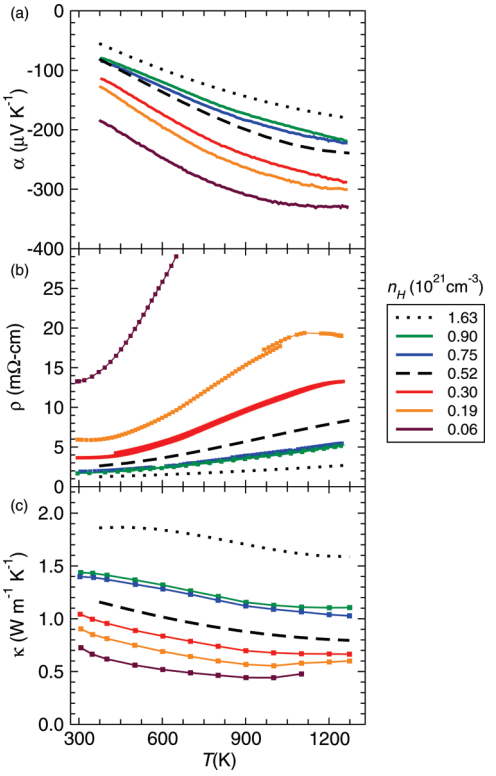

Figure 3. Temperature dependence of the transport properties in $La_{3-x-y}Yb_yTe_4$ (solid curves, filled markers) and $La_{3-x}Te_4$ (broken black curves): (a) Seebeck coefficient, (b) electrical resistivity, and (c) thermal conductivity. All panels use the same legend, which shows the room temperature Hall carrier concentrations. Table 1 can also be utilized to identify the compositions with Yb.

Also, divalent Yb has been suggested in $Pb_{1-x}Yb_xTe$ from lattice parameter data[17] and X-ray photoemission spectroscopy;[18] this is contrary to $Pb_{1-x}Yb_xS$ where mixed Yb valency is observed.[18] Thus, it is believed that Te is not electronegative enough to promote significant concentrations of Yb^{3+} and Yb can be regarded as Yb^{2+} in the lanthanum telluride matrix. Confirmation that Yb^{3+} does not exist in the matrix via magnetic measurements would be challenging due to the likely inclusion of magnetic impurities, as observed in $La_{3-x}Te_4$.[8]

The temperature dependence of the various transport properties is shown in Figure 3, where an increase in the magnitudes of α and ρ is observed with increasing T and decreasing n_H (increasing Yb content). For samples with the largest n_H, |α| increases linearly with increasing T, while those with low n_H manifest the detrimental effects of minority carrier activation at high T. Similar behavior is observed in the electrical resistivity, where the more heavily doped samples behave more like metals (linear increase with T) and those with lower doping act more like lightly doped semiconductors (ρ increases as $T^{1.5}$ until minority carrier activation is observed). The thermal conductivity decreases with increasing temperature and decreasing n_H (Figure 3b), as expected for heavily doped, crystalline semiconductors. Note the data for ρ of the more resistive sample were very difficult to obtain due to

(11) Gschneidner, K. A. *J. Less-Common Met.* **1969**, *17*, 13–24.
(12) Abrikosov, N. K.; Zinchenko, K. A.; Eliseev, A. A. *Inorg. Mater.* (*Engl. Transl.*) **1970**, *6*, 1021.
(13) Greenwood, N. N.; Earnshaw, A. *Chemistry of the Elements*; Pergamon Press: New York, 1984.
(14) Temmerman,W. M.; Petit, L.; Svane, A.; Szotek, Z.; Lüders, M.; Strange, P.; Staunton, J. B.; Hughes, I. D.; Gyorffy, B. L. *Handbook on the Physics and Chemistry of Rare Earths*; Elsevier: Oxford, 2009; Vol. *39*.
(15) Padalia, B. D.; Lang, W. C.; Norris, P. R.; Watson, L. M.; Fabian, D. J. *Proc. R. Soc. London, Ser. A* **1977**, *354*, 269–290.
(16) Hulliger, F. *Mater. Res. Bull.* **1979**, *14*, 259–262.
(17) Partin, D. L. *J. Appl. Phys.* **1985**, *57*, 1997.
(18) Golacki, Z.; Heinonen, M. *Acta Phys. Pol., A* **1997**, *91*, 775–778.

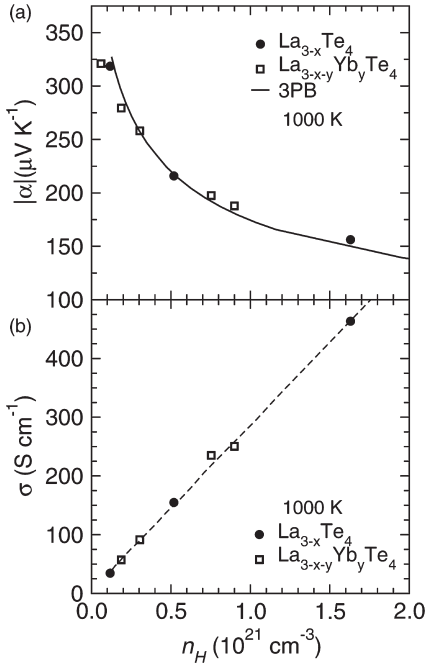

Figure 4. Dependence of (a) Seebeck coefficient and (b) electrical conductivity on the room temperature carrier density is found to be similar in $La_{3-x-y}Yb_yTe_4$ and pure $La_{3-x}Te_4$. The dashed curve in (a) is the semiempirical model taken from ref 5 for 1000 K, which utilizes three parabolic bands.

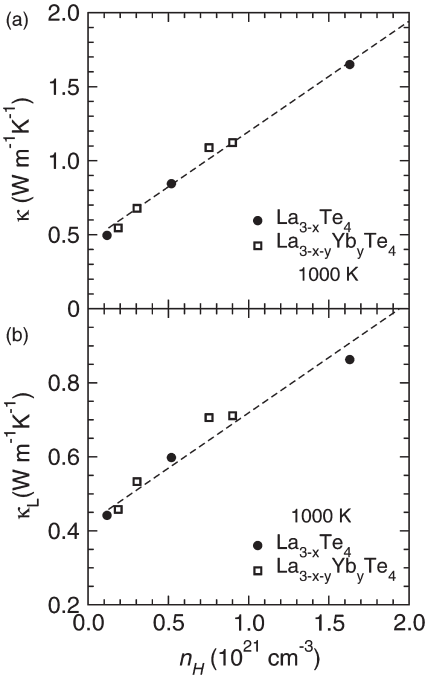

Figure 5. (a) Total and (b) lattice thermal conductivity versus room temperature Hall carrier density is similar in samples with and without Yb. The decrease in κ_L with decreasing n_H is associated with increasing point defect scattering.

rapid oxidation and poor quality contacts at this carrier concentration; efforts to obtain the high temperature ρ data were abandoned upon realization that this sample has a nonoptimal carrier density (see below).

To examine the influence of Yb on thermoelectric performance other than by changing n_H, the n_H dependence of α and the electrical conductivity ($\sigma = 1/\rho$) is examined in Figure 4, which shows data at 1000 K. The dependence α and σ on n_H is found to be similar in samples with and without Yb. Also, the band gap, estimated from the maximum in the Seebeck coefficient $E_g \sim 2e\alpha_{max}T_{max}$, is found to be ~0.8 eV in both types of samples.[1] These results suggest that the addition of Yb changes the transport properties through a modification of the carrier density alone and not through a change in the electronic structure. A single band model fails to capture the full n dependence of α in $La_{3-x}Te_4$, and thus the solid curve in Figure 4a is a three parabolic band (3PB) model taken from ref 5, where it is termed the "semiempirical multiparabolic band model".

Previous work on $La_{3-x}S_4$ revealed an increase in the thermoelectric power factor ($\alpha^2\sigma$) with substitutions of the form $La_{3-y}RE_yS_4$, where RE = Sm, Eu, and Yb.[9] This observed improvement was attributed primarily to enhancements in the Seebeck coefficient, which can be understood as changes in the effective mass. This is physically plausible, as the conduction band is dominated by lanthanum states[5,19] and thus a substitution for lanthanum may change the conduction band effective mass. If a similar change were to occur in the tellurium based system, $La_{3-x-y}Yb_yTe_4$, a deviation from the 3PB model in Figure 4a would have been observed. The absence of any obvious change to band structure suggests the Yb f-states reside below the valence band edge in lanthanum telluride. This generalization is consistent with the rigid assignment of Yb as Yb^{2+} in the telluride. However, the Yb−S phase diagram is complex and contains phases with Yb^{3+} (one unfilled f-state). Thus the improvement in $La_{3-y}Yb_yS_4$ may be related to a valence fluctuation that places f-states near the conduction band edge and promotes a larger effective mass. This may be viewed as similar to Tl doping in PbTe, which promotes an increased hole effective mass through the resonant impurity states associated with Tl.[20]

The dependence of thermal conductivity on n_H is shown in Figure 5b. The decrease in κ with decreasing n_H is common for semiconductors due to the decrease in the electronic contribution κ_e. However, even the lattice thermal conductivity κ_L decreases with decreasing n_H in $La_{3-x}Te_4$. The decrease in κ_L with decreasing n_H for pure $La_{3-x}Te_4$ is due to increasing point defect scattering as the La vacancy concentration increases.[1,8] The compositions selected for this study contain the additional point defect scattering associated with Yb, and thus the dependence of κ_L on n_H is similar in the Yb containing samples.

The lattice thermal conductivity was obtained by using a single parabolic band model to estimate the Lorenz number L under the assumption that acoustic phonon scattering limits the carrier mobility. Specifically, $L(T)$ is obtained via $\alpha(T)$ as both depend on only the

(19) Shim, J. H.; Kim, K.; Min, B. I.; Kang, J.-S. *Physica B* **2003**, *328*, 148–150.

(20) Heremans, J. P.; Jovovic, V.; Toberer, E. S.; Saramat, A.; Kurosaki, K.; Charoenphakdee, A.; Yamanaka, S.; Snyder, G. J. *Science* **2008**, *321*, 554–557.

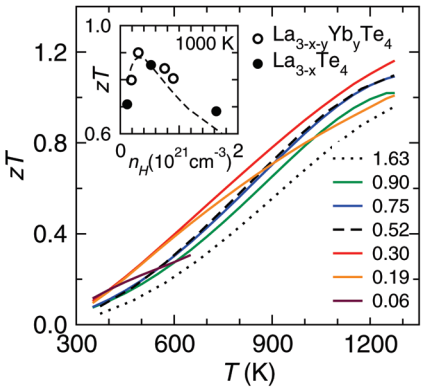

Figure 6. Temperature dependent thermoelectric figure of merit showing similar behavior in samples with Yb (solid curves) and without Yb (broken black curves). The inset shows zT at 1000 K versus carrier density with a curve generated from those shown in Figure 4 (α and σ) and Figure 5a for κ. The legend provides n_H values in units of 10^{21} cm^{-3}.

electrochemical potential and the energy dependence of the carrier relaxation time (when one scattering mechanism limits the carrier mobility). The Wiedemann−Franz relationship is then utilized to estimate $\kappa_e = L\sigma T$, which is subtracted from κ to obtain κ_L.[1]

The temperature dependence of the thermoelectric figure of merit zT is shown in Figure 6, where the legend again shows the room temperature values of n_H in units of 10^{21} cm^{-3}. The largest zT is observed in a Yb containing sample with $n_H = 0.30 \times 10^{21}$ cm^{-3}, which possesses zT near 1.2 at 1273 K and an average zT of 1 between 900 and 1273 K.

Prior work suggested an optimum doping level at $n_H \sim 0.9 \times 10^{21}$ cm^{-3}, and thus this work suggests lower values of n_H are desirable. The inset in Figure 6 examines this optimization at 1000 K, where the dotted curve has been generated using the 3PB model and linear fits in Figure 4a,b and Figure 5a. While the increase in zT is within the estimated error in zT, the agreement with the simple model shown supports the claim that an optimum exists near $n_H \sim 0.3 \times 10^{21}$ cm^{-3}. Also, the wide range of compositions supporting average zT near unity is promising for device development. We note that similar zT values should be possible without the addition of Yb but that the presence of Yb allows such compositions to be probed more readily.

Conclusion

The substitution of Yb for La has facilitated the optimization of thermoelectric efficiency in an *n*-type material with one of the highest known thermoelectric efficiencies above 1000 K. The relationship between composition and experimental carrier density suggests that Yb is divalent when substituted for La, and thus a threefold improvement in the chemical control of carrier density can be obtained. After examining a series of samples with near optimal n, a maximum zT is predicted and obtained at $n_H \sim 0.3 \times 10^{21}$ cm^{-3}, where $zT \sim 1.2$ was observed at 1273 K. Continued efforts to understand and enhance thermoelectric transport in $La_{3-x}Te_4$ can utilize Yb substitution to examine the relationship between mobility and lattice thermal conductivity, particularly in vacancy free samples.

Acknowledgment. This work was performed at the Jet Propulsion Laboratory and California Institute of Technology under contract with the National Aeronautics and Space Administration. The authors thank L. Danielson for useful discussions. The authors also thank L.D. Zoltan for assistance with Seebeck coefficient measurements and T. Ikeda for assistance with WDS measurements.